Physica B 650 (2023) 414554

Contents lists available at ScienceDirect

Physica B: Condensed Matter

journal homepage: www.elsevier.com/locate/physb

Structural, electronic, magnetic, and optical properties of Fe-doped $Na_2ZnP_2O_7$ host: *ab-initio* calculation

Houssam Eddine Hailouf [a,*], L. Gacem [a], A. Gueddim [a], Ali H. Reshak [b,c,d], K.O. Obodo [e,f], B. Bouhafs [g]

[a] Materials Science and Informatics Laboratory, Faculty of Science, University of Djelfa, 17000, Djelfa, Algeria
[b] Physics Department, College of Science, University of Basrah, Basrah post code 61004, Iraq
[c] Center of Excellence Geopolymer and Green Technology (CEGeoGTech), University Malaysia Perlis, 01007 Kangar, Perlis, Malaysia
[d] Department of Instrumentation and Control Engineering, Faculty of Mechanical Engineering, CTU in Prague, Technicka 4, 616607 Prague, Czech Republic
[e] HySA Infrastructure Centre of Competence, Faculty of Engineering, North-West University, Private Bag X6001, Potchefstroom, 2531, South Africa
[f] National Institute of Theoretical and Computational Sciences, Johannesburg 2000, South Africa
[g] Laboratoire de Modélisation et Simulation en Sciences des Matériaux, Université Djillali Liabès de Sidi Bel-Abbès, Sidi Bel-Abbès, 22000, Algeria

ARTICLE INFO

Keywords:
Diphosphate
Transition metal doping
GGA+U
Energy defect level
Magnetic properties

ABSTRACT

Recent experiments on the optical characterization of transition metal ions doped $Na_2ZnP_2O_7$ host lattice, show promise as luminescent materials. A detailed study using *ab-initio* DFT-based calculations to understand how the properties of the $Na_2ZnP_2O_7$ host lattice are affected by the Fe dopants is carried out. The GGA and GGA + U functionals were used to determine the electronic and optical properties of the host lattice and Fe ion doped $Na_2ZnP_2O_7$. Full structural geometric optimization was performed for pristine $Na_2ZnP_2O_7$ host lattice, super-cell and Fe doped super-cell. The computed electronic band structure, density of states, and dielectric functions for the pristine and doped crystal structure reveal changes due to the Fe dopant ion, which induces various states within the band gap of $Na_2ZnP_2O_7$ lattice. The total magnetic moment of the host lattice is found to be zero, which implies nonmagnetic behavior as shown by the spin-polarized band structure, while the spin-polarized band structure of the Fe-doped $Na_2ZnP_2O_7$ structure shows a ferromagnetic character. This study provides new clues about the diphosphate compounds with transition metal dopant ions.

1. Introduction

The diphosphate compounds have a chemical formula $AREP_2O_7$ (A = alkali metal, RE = rare earth metal). This class of materials possess a wide band gap, which provide host for rare earth and transition metal ions. Also, multiple defects level can be incorporated in their forbidden gap, trapping electrons and holes and causing radiative recombination [1,2]. The wide band $Na_2ZnP_2O_7$ compound have sparked significant interest with considerable attention focused on the development of luminescent materials. This is due to their exceptional adaptability, charge, and the local environment symmetry, which allows for the selective tuning of properties. The large number of $AREP_2O_7$ compounds as well as the possibilitiy of isomorphic substitution makes thempotentially applicable in optical amplification, optical data storage, white light-emitting diodes (w-LEDs), solid-state laser materials, up-conversion, gamma, X-ray scintillators, etc. [3–9]. Furthermore, the diphosphate-based compounds have several advantages for industrial use; they are strong candidates for immobilizing hosts for nuclear waste [10], have high catalytic performance [11], as well as other relevant industrial applications [12–15].

Fundamentally, these $AREP_2O_7$ compounds are very important sources of light. These compounds are appropriate for doping with multiple lanthanide and metal ions leading to changes in the electronic and optical properties [16]. This results in improvement of their applicability in lighting and display devices. Experimental investigations have been carried out on the photo-physical properties of $AREP_2O_7$ compound by doping with various lanthanide and metals ions as activators. These ions have a specific optical characteristic when introduced into a host lattice and opens the path for the future growth of optical amplifiers and phosphors. The optical impact of lanthanide ions is takes advantage of electronic transitions possible due to the partially filled 3*d* and 4*f* energy shells of transition metal and rare-earth ions [17,18].

* Corresponding author.
E-mail address: h.hailouf@yahoo.com (H.E. Hailouf).

https://doi.org/10.1016/j.physb.2022.414554
Received 20 July 2022; Received in revised form 25 November 2022; Accepted 2 December 2022
Available online 3 December 2022

Currently, there are efforts by various researchers on the photon-electron conversion efficiency to replace traditional renewable energy approaches, such as the application of a solid-state perovskite device constructed by the mesoporous architecture [19], Shahid Hussain et al. [20,21] used the X-ray technique to conduct a thorough examination of these porous structures, and their results suggest possible uses as electrocatalysts and energy storage systems.

In the last few decades, several studies have been published on the changes and effect of different properties of diphosphates-based compounds when doped with different lanthanide and metals ions [7,22,23]. According to our understanding, theoretical studies of crystal structure engineering and solid comprehension of electronic band structures of the diphosphates host lattice, and the effects of dopant atoms on the stability, structural, electronics and optical properties have a long way to go in terms of the technological applications. To the best of our knowledge, no theoretical study on the Fe doped diphosphates compounds have been performed to date. The aim of this paper is to provide a deeper understanding of the electronic and optical features attributed to Fe dopants ions in the $Na_2ZnP_2O_7$ host lattice. Thus, we employed ab initio technique based on density functional theory (DFT) to explore the atomic structures, formation energies, electronic structures and optical properties of the Fe-doped $Na_2ZnP_2O_7$ host lattice. To overcome the limitation of standard density functional leading to the underestimation of the band gap, the Generalized Gradient Approximation (GGA) with a Hubbard U approach is employed, which can provide a better description by computing the Hubbard U parameter [24].

2. Theoretical approach and computational method

In the present study, we have carried out DFT calculations with spin polarization expanded in plane-wave Quantum ESPRESSO package [25] with both ultra-soft [26] and norm-conserving Vanderbilt [27] pseudopotentials to describe electron-ion interactions [28] executed on pristine and various ions doped $Na_2ZnP_2O_7$. The valence electrons for the considered elements are Na: $3s^1$, Zn: $4s^23d^{10}$, P: $3s^23p^3$, O: $2s^22p^4$, and Fe: $4s^23d^6$. We applied the exchange correlation GGA-PBE functional [29] for the structural optimization and energetic properties in the ground state. The kinetic energy cutoff was set at58 Ry and 580 Ry for the charge density. The convergence criteria were set to $1. \times 10^{-8}$ eV for the total energy calculations.

The crystal structure and stability were determined, followed by the electronic and optical properties of the host lattice and various ions doped $Na_2ZnP_2O_7$ computed using GGA-PBE + U functional [24]. We used the linear response approach indicated by Cococcioni et al. [30] to calculate the Hubbard U parameter added on the O $2p$ as well as the $3d$ and $4f$ of dopants orbitals in a self-consistent trend as implanted in Quantum-Espresso package with respect to staying away from empirical estimation, the obtained values U = 4.81, 3.38 and 7.1, to treat, respectively, O $2p$, Fe $3d$ and Zn $3d$ orbitals.

The full structural optimization of the $Na_2ZnP_2O_7$ compound with 48 atoms in the unit cell as presented in Fig. 1 was carried out employing the Broyden–Fletcher–Goldfarb-Shanno (BFGS) method [31] and a Monkhorst-Pack [32] grid of $6 \times 6 \times 4$. The significant component of the Hellmann-Feynman forces acting on single atom was set to be lower than $1. \times 10^{-8}$ eV/Å for energy convergence criteria. The electronic and optical properties were computed by using denser Monkhorst-Pack grid of $10 \times 10 \times 8$.

To model the doped systems, we considered a $2 \times 2 \times 1$ supercell from the $Na_2ZnP_2O_7$ primitive cell as presented in Fig. 1 with 192 atoms (Na = P = 32 atoms, Zn = 16 atoms and O = 112 atoms, the amount of doping is 6.25% for both systems). In this study, the one Fe atom was used to substitutionally replace Zn atom in the $Na_2ZnP_2O_7$ supercell. For the one Fe atom replacing Zn atom, there are 16 different possible configurations, and crystal structure optimization was ran for each configuration with the structure having the lowest formation energy determined as the best doping positions amongst all possible configurations. A $1 \times 1 \times 2$ Monkhorst-Pack grid was used for the k-point to sample reduced Brillouin zone (BZ) for the total energy and atomic relaxation calculations incorporating the same as primitive cell convergence criteria.

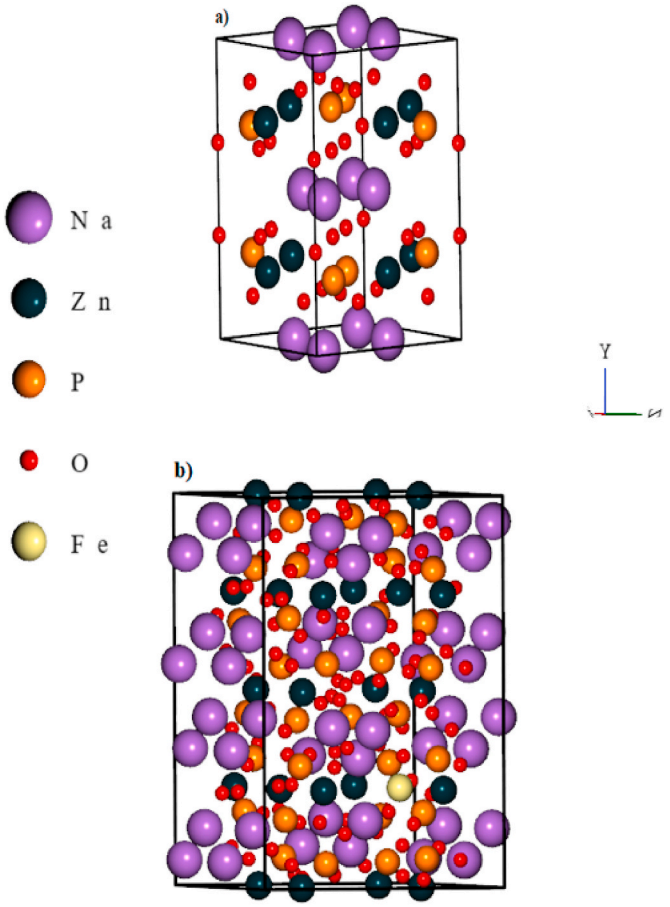

Fig. 1. Optimized crystals structures of (a) pure $Na_2ZnP_2O_7$ host lattice and (b) Fe-doped $Na_2ZnP_2O_7$ using GGA-PBE.

3. Results and discussion

3.1. Structural properties and energetic

The crystal structure of the $Na_2ZnP_2O_7$ host lattice consists of 48 atoms with four formula units per cell, crystallized in a tetragonal structure with the space group $P4_2/mnm$ (136) as depicted in Fig. 1(a). The host lattice has ZnO_4 tetrahedral linking corners with four similar P_2O_7 and Na atom placed between the layers [33] containing seven nonequivalent atoms, two Na atoms (Na1 and Na2), one zinc atom (Zn1), one phosphorus atom (P1) and three oxygen atoms (O1, O2 and O3). The corresponding Wyckoff positions are 4*f*, 4*g*, 4*d*, 8*j*, 4*e*, 8*j*, and 16*k*.A basic agreement of the atomic positions with available theoretical and experimental results are found as shown in Table 1. Full geometrical optimization was performed for the $Na_2ZnP_2O_7$ host lattice, $Na_{32}Zn_{16}P_{32}O_{112}$ super-cell and $Na_2Zn_{0.937}Fe_{0.0625}P_2O_7$ doped super-cell. An overall agreement of the calculated crystal parameters (a, c) of the host $Na_2ZnP_2O_7$ tetragonal structure with available theoretical and experimental results [23,33,34] is found as illustrated in Table 2.

Based on the calculated host lattice, a large super cell of 192 atoms was optimized to study the presence of Fe dopants ions in the host lattice $Na_2Zn_{1-x}Fe_xP_2O_7$ as shown in Fig. 1. From the optimized lattice constants of the doped compound presented in Table 2, it is observed that the Fe doped $Na_2ZnP_2O_7$ host lattice results in small volume increase,

Table 1
The calculated GGA-PBE atomic positions of $Na_2ZnP_2O_7$ compound. Theoretical and experimental values are included for comparison.

Atom	Wyckoff site	Present			Other calc [33].			X-ray diffraction [9]		
		x	*y*	*z*	*x*	*y*	*z*	*x*	*y*	*z*
Na_1	4*f*	0.694	0.694	0.5	0.688	0.688	0.5	0.697	0.697	0.5
Na_2	4*g*	0.645	0.645	0	0.649	0.649	0	0.639	0.639	0
Zn_1	4*d*	0	0.5	0.25	0	0.5	0.25	0	0.5	0.25
P_1	8*j*	0.138	0.138	0.288	0.14	0.14	0.291	0.133	0.133	0.209
O_1	4*e*	0.136	0.136	0.345	0.138	0.138	0.357	0.132	0.132	0.354
O_2	8*j*	0.08	0.30	0.143	0.081	0.309	0.138	0.086	0.303	0.152
O_3	16*k*	0.5	0.5	0.643	0.5	0.5	0.642	0.538	0.538	0.660

Table 2
The computed lattice constants *a* and *c* (in Å), volume *V* (in $Å^3$) and formation energy E^f (in eV/atom) of the $Na_2ZnP_2O_7$ host and Fe ions doped $Na_2ZnP_2O_7$ lattice using GGA-PBE compared to other theoretical and experimental studies.

Compound	Ref.	*a*	*c*	*V*	E^f
$Na_2ZnP_2O_7$	Present	7.82	10.40	635.98	−15.85
	Other calc [33].	7.75	10.20	612.63	
	Expt [23].	7.74	10.50	629.20	
	Expt [34].	7.74	10.42	625.40	
$Na_2Zn_{0.937}Fe_{0.0625}P_2O_7$		7.77	10.44	632.10	−0.28

attributed to the ionic radii of Zn being close to the Fe. Also little change in the lattice parameters and no significant major lattice distortion are apparent after Fe doping at Zn site in $Na_2ZnP_2O_7$ host lattice.

The formation energy is an important criterion to confirm the relative stability of a compound and for dopants in the host lattice, the formation energies per atom of each system is calculated through the following equations [17]:

$$E^f_{Na_2ZnP_2O_7} = E^t_{Na_2ZnP_2O_7} - (\mu_{Na} + \mu_{Zn} + \mu_P + \mu_O) \quad (1)$$

$$E^f_A = E^t_{doped} - E^t_{perfect} + (\mu_{Zn} - \mu_A) \quad (2)$$

Where $E^t_{Na_2ZnP_2O_7}$ is the total energy of the pure $Na_2ZnP_2O_7$ host lattice, and μ_{Na}, μ_{Zn}, μ_P and μ_O are the chemical potential of Na, Zn, P and O_2 molecule, respectively. E^f_A is the formation energy of each corresponding system under consideration, this energy (E^f_A) is the amount of energy required to substitutionally replace the Zn ion with the dopant ion. The lower the formation energy, the easier it is for the dopants atom to be incorporated into the $Na_2ZnP_2O_7$ host lattice. E^t_{doped} and $E^t_{perfect}$ are the total energy of the doped and perfect undoped supercell, respectively. μ_A denotes the chemical potential of the corresponding dopant ion.

The calculated formation energy of the undoped and all doped systems is presented in Table 2. The formation energy of the pure $Na_2ZnP_2O_7$ host lattice and Fe doped $Na_2ZnP_2O_7$ are found to be negative. This means that the formation of this $Na_2ZnP_2O_7$ host lattice is possible from its elemental constituents and Fe-doped $Na_2ZnP_2O_7$ is feasible to realize.

3.2. Electronic properties

The electronic band structure and density of states (DOS) of a compound is highly significant because it is provided important information about the nature of the compound, *i.e.*, conductor, semiconductor, insulator, and the possible inter-electronic state transitions [35,36].

3.2.1. The band structure of pure and Fe-doped $Na_2ZnP_2O_7$

To examining the band gap of the pure $Na_2ZnP_2O_7$ host lattice, we computed the electronic band structure by using the GGA-PBE + *U* approximation. The Hubbard *U* parameter was applied on O-2*p* and Zn-3*d* states of the pure $Na_2ZnP_2O_7$ host lattice. Fig. 2 shows both the valence band maximum (VBM) and the conduction band minimum

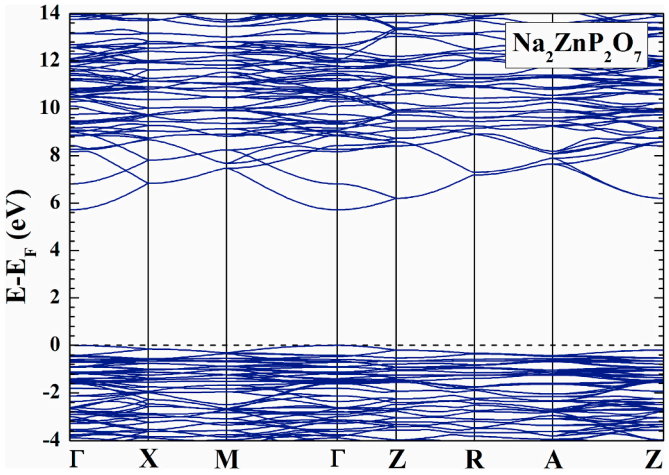

Fig. 2. The electronic band structure of pure $Na_2ZnP_2O_7$ host lattice calculated via GGA-PBE + *U*. The horizontal dashed line indicates the Fermi level, which is set at the valence band maximum.

(CBM) are situated at the Γ point ($\Gamma_v \rightarrow \Gamma_c$) of the BZ, which confirms the direct band gap nature of the pure $Na_2ZnP_2O_7$ host lattice. The computed band gap value of the host lattice is about 5.7 eV, which agrees with our previous theoretical studies [33]. There is no experimental data on the electronic band gap of the $Na_2ZnP_2O_7$ compound available in the literature. The calculated band gap value implies that the $Na_2ZnP_2O_7$ compound has a wide band gap, and it can appropriately accommodate both the ground and excited states of the impurity energy levels within the band gap for use as a luminescent host lattice. Fig. 2 shows that the conduction band states exhibit pronounced dispersion along all paths in the BZ, whereas the valence band states are relatively flat, especially at the top of the valence band. This indicates that the holes have very limited mobility.

The spin-polarized band structure (see Fig. 3(a) for spin-up and Fig. 3 (b) for spin-down) of incorporating of Fe ion $Na_2ZnP_2O_7$ host lattice is presented. The presence of one Fe ion substitutionally replacing the Zn ion shifts the Fermi level (E_F) from the top of the VB to the bottom of the CB. This shift of the E_F shows the *n*-type doping nature of Fe in $Na_2ZnP_2O_7$ lattice. is effectively affected by incorporating impurity states below the conduction band because of the Fe doping, it can be seen in Fig. 3. In the spin up case, nearly flat bands of the Fe 3*d* states are obtained in the host's band gap with the energy state being about 0.42 eV above the VBM. This implies a high degree of localization of these states around the Fe ions. The Fe 3*d* states within the band gap of $Na_2ZnP_2O_7$ reveals itself in the optical behavior as well. Thus, the impurity energy levels act as the acceptor to spatially separate the photogenerated electrons from holes and favor the photon absorption. From Fig. 3(b), the spin down case, there is a formation of an impurity state between the band-gap regions. The Fe 3*d* impurity states appear within the $Na_2ZnP_2O_7$ band gap. The lowest state is about 2.4 eV above the top of the VB and two uppermost impurity states located at about 0.5 eV below the CBM. The impurity states above the VBM as well as below the

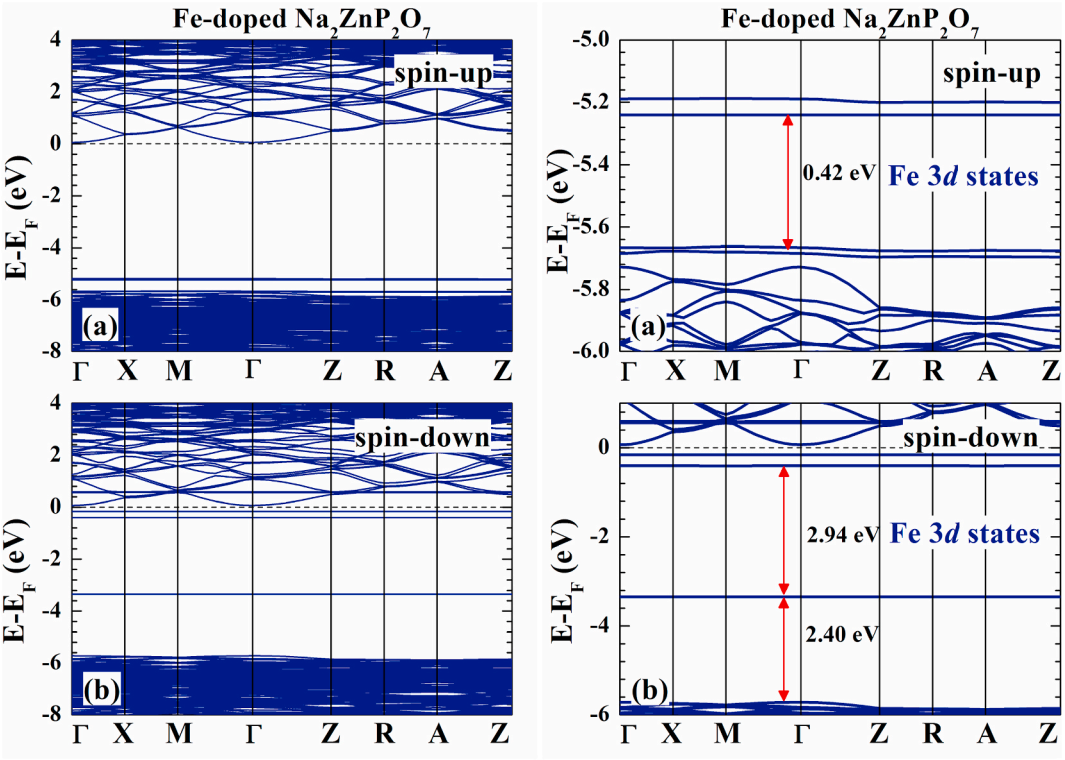

Fig. 3. The electronic band structure for (a) spin up and (b) spin down of Fe-doped $Na_2ZnP_2O_7$ calculated via GGA-PBE + U. The horizontal dashed line indicates the Fermi level, which is set at the zero level.

CBM simultaneously could serve as electron-hole recombination centers; therefore Fe-doped $Na_2ZnP_2O_7$ will enhance visible light photocatalytic activity.

3.2.2. *The density of states of pure and Fe-doped $Na_2ZnP_2O_7$*

To explore the individual orbital contribution in the band structure of pure $Na_2ZnP_2O_7$ host lattice, the total and partial densities of states (TDOS and PDOS) for Na, Zn, P and O atoms are calculating using GGA-PBE + U, as illustrated in Fig. 4. It is seen from the TDOS that the valence band ranges from −8 to 0 eV of $Na_2ZnP_2O_7$ host is completely occupied, which consist mainly of the O 2p and Zn 3d states and a minor contribution of the mixed states P-3p and Na-3p, whereas the VBM closet to the Fermi level is formed by the O 2p states. The conduction band ranges from 5.7 to 14 eV has significant contribution from P-3p and Na-3p states with a minor contribution from the 3s and 3p states of P, O and Zn, which arises owing to the consequences of hybridization.

The main contribution to the different orbitals of the atoms in the calculated bands structure for spin up and spin down can be explained considering the TDOS and PDOS as shown in Fig. 5. We observed in Fig. 5(a) that the TDOS has a valence band of about 10 eV in width, namely from −16 to −6 eV and consists of three sub-bands. The lower bands from about −15.5 eV to −14.5 eV is formed by the O and P 2p states, and the middle bands is from about −13 eV to −11 eV is formed by the Zn 3d states with minor contribution of O 2p states, whereas the upper states from approximately −11 eV to −6 eV is due to the O 2p states. The conduction band, which is about 4 eV wide, is composed of the P 3p and Na 3p states, to which the Zn 3d and O 2p states have a small contribution. From the PDOS, the impurity states in the band gap are mainly composed of Fe 3d states.

To study the local and total magnetic moment of the Fe-doped $Na_2ZnP_2O_7$ host lattice, spin polarized DFT calculations with GGA + U functional were employed. The total magnetic moment of the $Na_2ZnP_2O_7$ host lattice is found to be zero. The non-magnetic behavior is verified from the spin-polarized band structure, which shows that the spin up and spin down configuration are symmetric. Thus, the ground state of the host is non-magnetic, while the profile of the spin-polarized band structure of the Fe-doped $Na_2ZnP_2O_7$ host (see Figs. 2 and 3) shows ferromagnetic character. From PDOS, we can see that the electronic state has a significant impact on magnetic characteristics. We found that the s-states of Fe have a little effect, whereas the 3d states of Fe contribute significantly to magnetism. It is further observed that the total magnetic moments of the Fe-doped $Na_2ZnP_2O_7$ host lattice is approximately $4\mu_B$, and the magnetic moment per single Fe atom was about $3.3825\mu_B$. The highest magnetic moment in all super-cells is related to the Fe atom, which accounts for around 85% of the total magnetic moments observed.

The variation of the band structure for the pristine $Na_2ZnP_2O_7$ host lattice and Fe doped structure signifies charge transfer. Theoretical calculation for the 3D charge density difference (CDD) as presented in Fig. 6 was carried out to provide visual evidence of charge transfer. The 3D charge density difference was plotted by subtracting the charge density of the doped supercell from that of the perfect supercell. Electron depletion and accumulation occurred on the FeO_4 tetrahedral site due to the Fe dopant ions in the defect supercell. The yellow color represents positive electronic densities which accept electrons, and the cyan color represents negative densities which donate electrons. Accumulated negative and positive charges, respectively is indicative of the strong bond formation with some covalent character.

3.2.3. *The optical properties of pure and Fe-doped $Na_2ZnP_2O_7$*

The optical properties of diphosphates-based compound are calculated, which is applied to understand the luminescent and photocatalytic materials. The diphosphates-based compound is important for optoelectronic devices. When photons are absorbed or emitted, electron transitions between occupied and unoccupied states can occur, considering single-particle excitations and Plasmon's. To evaluate the optical properties of pristine $Na_2ZnP_2O_7$ lattice and the influence of the Fe dopants on the optical behavior of $Na_2ZnP_2O_7$ host lattice. The complex

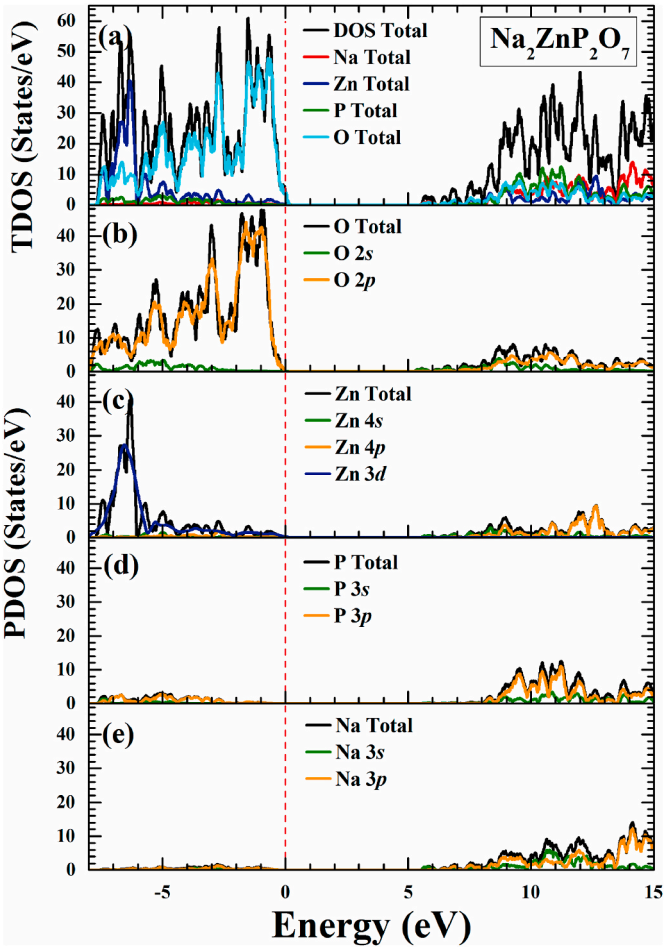

Fig. 4. The calculated (a) total densities of states (DOS) and partial densities of states (PDOS) of $Na_2ZnP_2O_7$ host lattice via GGA-PBE + U with contributions of the (b) O atoms, (c) Zn atoms, (d) P atoms and (e) Na atoms.

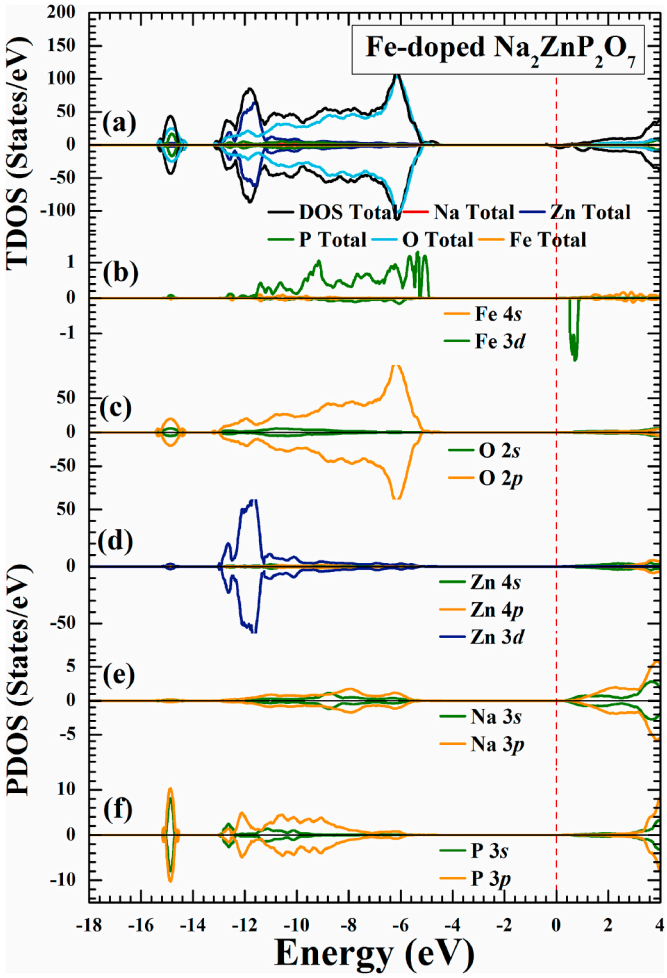

Fig. 5. The calculated (a) total densities of states (DOS) and partial densities of states (PDOS) of Fe-doped $Na_2ZnP_2O_7$ host lattice via GGA-PBE + U with contributions of the (b) Fe atom, (c) O atoms, (d) Zn atoms, (e) Na atoms and (f) P atoms.

dielectric function of a solid is calculated as given in equation (3):

$$\varepsilon(\omega) = \varepsilon_1(\omega) + i\varepsilon_2(\omega) \tag{3}$$

The real (ε_1) and imaginary parts (ε_2) both parts are connected by the Kramers-Kronig formula [37,38]. The refractive index $n(E)$, the extinction coefficient $K(E)$, the absorption coefficient $\alpha(E)$, the reflectivity $R(E)$, and the energy-loss spectrum $L(E)$ formulae are presented below [17,39].

$$n(E) = \left[\frac{\sqrt{\varepsilon_1(E)^2 + \varepsilon_2(E)^2} + \varepsilon_1(E)}{2}\right]^{\frac{1}{2}} \tag{4}$$

$$k(E) = \left[\frac{\sqrt{\varepsilon_1(E)^2 + \varepsilon_2(E)^2} - \varepsilon_1(E)}{2}\right]^{\frac{1}{2}} \tag{5}$$

$$\alpha(E) = 2\omega k(E) \tag{6}$$

$$R(E) = \frac{[n(E)-1]^2 k(E)^2}{[n(E)+1]^2 k(E)^2} \tag{7}$$

$$L(E) = \frac{\varepsilon_2(E)}{\varepsilon_1(E)^2 + \varepsilon_2(E)^2} \tag{8}$$

In this section, the optical properties of pristine and Fe doped $Na_2ZnP_2O_7$ were investigated using the DFT + U approach. The tetragonal symmetry is used for the $Na_2ZnP_2O_7$ host lattice, the components ε_x and ε_z dielectric function in the x and z directions, respectively, are employed to compute the dielectric tensor.

Fig. 7 show the variation of the real $\epsilon_1(\omega)$ and imaginary $\epsilon_2(\omega)$ part of the dielectric function ranging from 0 eV up to 25 eV, which is related to the optical response of the compound at all photon energies. The absorptive part $\epsilon_2(\omega)$ of dielectric function show that the optical absorption edge occurred at around 6 eV which is closely related to the band gap value obtained in our study, after that there is a broad peak for ε_{2x} and ε_{2z} direction at 12 eV and 11 eV, respectively, these peaks correspond to the absorption behavior of the electronic band structure of the compound which is related to the optical transitions from the valence band to the conduction band, that is consistent with our previous study [33]. Also Fig. 7(b) show an optical anisotropy of these two directions over the whole energy range.

Fig. 7(a) show the variation of the dispersive spectra of the dielectric function as the energy stored in compound, the two directions ε_{1x} and ε_{1z} increases from the low energy range, then it decays to zero at higher energy. This shows that the compound would not interact with high energy photons and thus transparent. At the zero-energy limit, the magnitude of the dielectric functions, $\varepsilon_1(0)$ is equal to 2.2. These static values are strongly correlated to the semiconductor's band gap, as discussed by Penn's model [33,40].

Fig. 7 (right panel) show the calculated real and imaginary parts of dielectric function for the Fe-doped $Na_2ZnP_2O_7$ host lattice. There is a

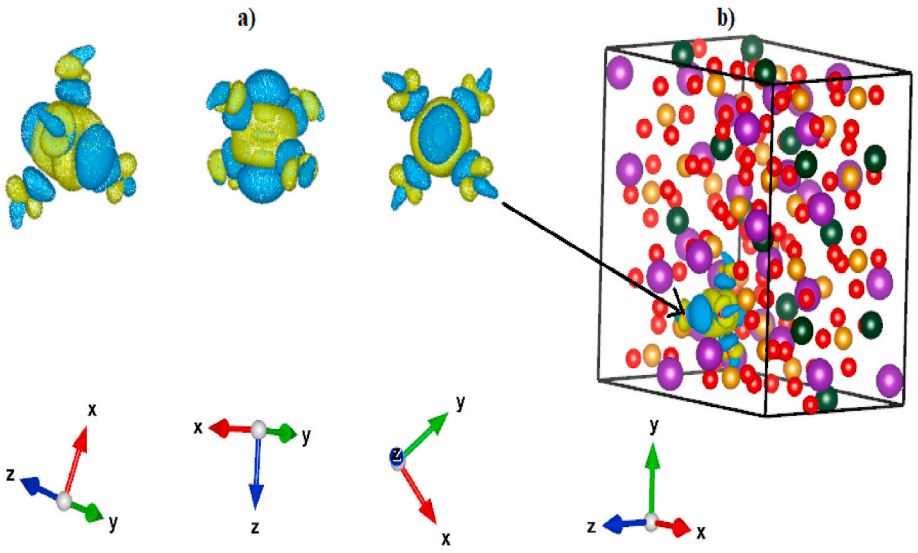

Fig. 6. The calculated charge density difference (CDD) of Fe-doped $Na_2ZnP_2O_7$ host lattice via GGA-PBE + U.

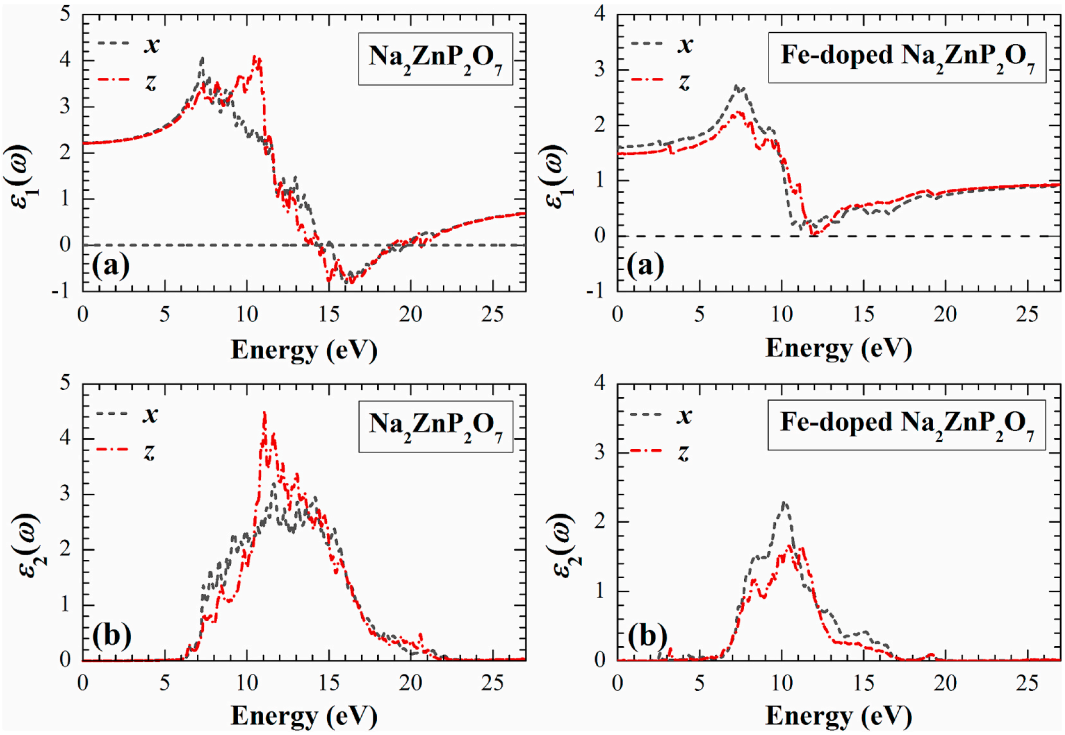

Fig. 7. The calculated dispersion of the (a) real $\epsilon_1(\omega)$, and (b) imaginary $\epsilon_2(\omega)$ parts of the dielectric function as a function of photon energy of pure $Na_2ZnP_2O_7$ host lattice (left panel) and Fe-doped $Na_2ZnP_2O_7$ (right panel) using GGA-PBE + U.

significant difference between Fig. 7 (left panel) and 7 (right panel). This difference arises from the change in the electron band structures. The peaks in the spectra are attributed to various electronic excitations from the occupied states in the valence band to the unoccupied states in the conduction band. Compared to the $Na_2ZnP_2O_7$ host lattice, the peaks in the spectra of Fe-doped $Na_2ZnP_2O_7$ compound shift towards the lower energy region from UV to visible and IR regions. Fig. 7(b) shows the absorptive part $\epsilon_2(\omega)$ of dielectric function. There is a small absorption peak in low energy region at about 2–3 eV. This reveals a new and separate pathway for the absorption of photons with energy lower than the gap width of the $Na_2ZnP_2O_7$ host lattice. The maximum value of $\epsilon_2(\omega)$ appears to be at 2.38 and 1.6 eV for x and z direction respectively, whereas highest peak for host lattice is reached at 3.2 and 4.5 eV for x and z direction respectively. The variation of the dispersive spectra of the dielectric function versus energies is shown in Fig. 7(a). This shows positive values of dispersion across all spectral ranges, whereas the dispersion curve of the host lattice shows negative values in the energy region 15–18 eV. We found that the magnitude of the dielectric functions $\epsilon_1(0)$ of Fe-doped $Na_2ZnP_2O_7$ is equal to 1.6 and 1.5 eV for x and z direction respectively, which is higher compared with the $Na_2ZnP_2O_7$ host lattice as shown in Fig. 7(a).

The calculated absorption coefficient of pure $Na_2ZnP_2O_7$ host lattice is shown in Fig. 8(a). We notice that the absorption edge rises from about 6 eV, which corresponds to the direct $\Gamma - \Gamma$ transition. The absorption

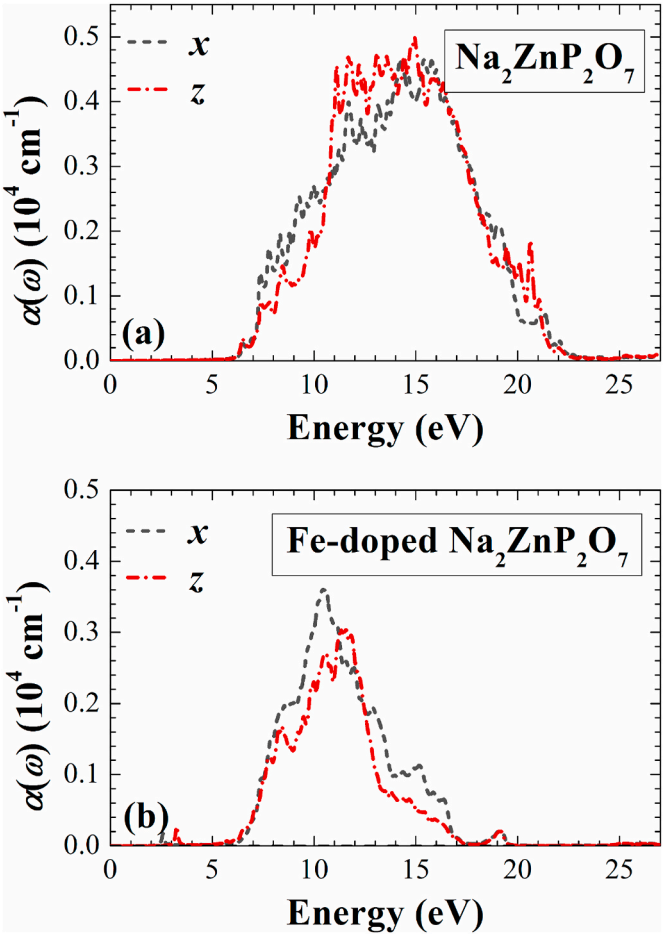

Fig. 8. The calculated optical absorption coefficient $\alpha(\omega)$ as a function of photon energy of (a) pure $Na_2ZnP_2O_7$ host lattice, and (b) Fe-doped $Na_2ZnP_2O_7$ using GGA-PBE + U.

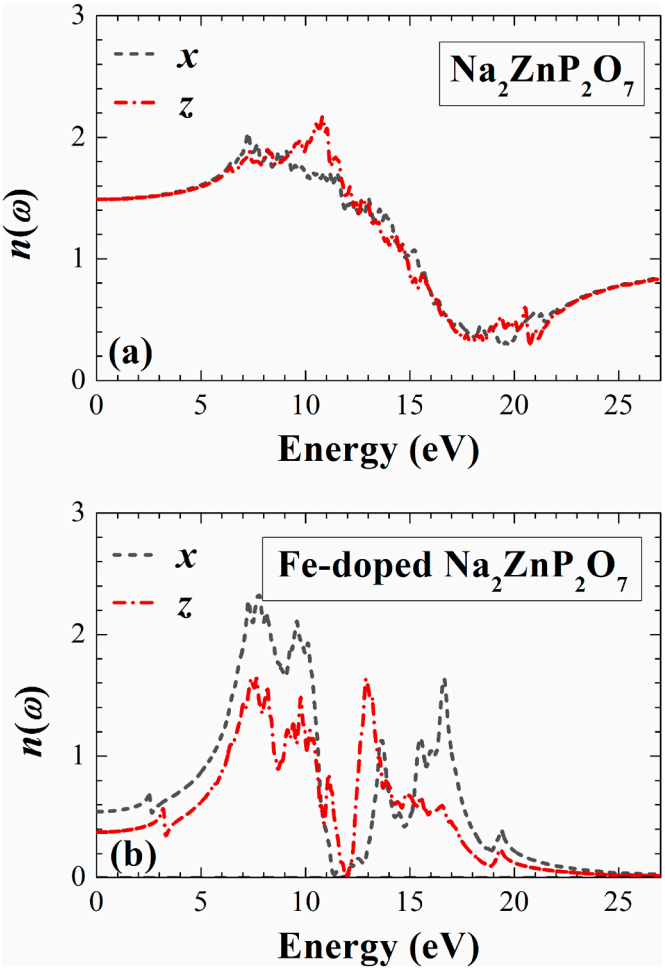

Fig. 9. The calculated dispersion of the refractive index $n(\omega)$ as a function of photon energy of (a) pure $Na_2ZnP_2O_7$ host lattice, and (b) Fe-doped $Na_2ZnP_2O_7$ using GGA-PBE + U.

continues to increase until reaching the maximum at 15 eV, this energy range lies within the UV range of the solar spectrum. Thus, this implies that there is medium photon absorption in the UV region. The results of optical absorption spectra of Fe-doped $Na_2ZnP_2O_7$ host lattice are illustrated in Fig. 8(b). Absorption spectra are assessed by considering energy in the range 0–25 eV. This is interpreted as the absorption range is very wide, which are from infrared to ultraviolet region.

These spectra presented as an effect of electrons excitations from valence to conduction band [41] and owing to quantum confinement effects, which are amplified by doping [42,43]. Quantum confinement effect is also responsible of narrower absorption width and the shifting of absorption maxima toward region of lower energies as compared to $Na_2ZnP_2O_7$ host lattice, which those phenomena can be ascribed to a red shift and considerable band gap reduction.

Fig. 9(a) shows the behavior of refractive index spectrum as a function of the energy of pure $Na_2ZnP_2O_7$ host lattice. The calculated refractive index is obtained with respect to the crystal structure axes of the compound. The static index for both x and z direction is $n\,(0) = 1.45$, which is in good agreement with the literature report [33,44]. The low value of the static index is a good indication that pure $Na_2ZnP_2O_7$host lattice is transparent. The calculated refractive index spectrum versus energy for Fe doped $Na_2ZnP_2O_7$host lattice is shown in Fig. 9(b). At zero energy, the refractive index $n(0)$ of Fe-doped $Na_2ZnP_2O_7$ is 0.5 and 0.4 for x and z direction, respectively, which is lower than the refractive index of the pure $Na_2ZnP_2O_7$ host lattice.

This is determined to be 1.45; this decrease in the static refractive index confirms the decrease in the band gap. This is due to enhanced photon scattering by crystal defects caused by the Fe dopants [45]. The lowest value of the absorption energy corresponds to the highest value of the refractive index. The refractive index starts decreasing when the absorption value increases, as seen in Fig. 9(b).

Fig. 10(a) depicts the extinction coefficient of pure $Na_2ZnP_2O_7$ host lattice which defines the absorption phenomenon in the complex refractive index. At an energy that corresponds to the optical band gap, the extinction value increases then falls to zero. This threshold is equal to 6 eV.

The extinction coefficient of Fe doped $Na_2ZnP_2O_7$ host lattice is illustrated in Fig. 10(b) with sharp peaks observed at 10 eV and 11 eV for x and z directions respectively. This lower energies result in better values of absorption and extinction coefficient (K).

In Fig. 11(a), the calculated reflectivity (R) of pure $Na_2ZnP_2O_7$ host lattice is presented. The reflection coefficient represents the amount of energy reflected in relation to the incident energy. The static value of the reflection coefficient is 0.15 for both x and z directions. The reflection coefficient increases then approaches the maximum values around the UV range at 12 eV for both the x and z direction. We showed a maximum transmittance (T) ($R \approx 0$, $T \approx 1$) as the compound is transparent without any absorption. The maximum transmittance (T) in pure $Na_2ZnP_2O_7$ host lattice is located at 17 eV.

Fig. 11(b) shows the calculated reflectivity (R) of Fe-doped $Na_2ZnP_2O_7$ host lattice, in which a sharp peak is obtained at lower energy. The doped structure shows a narrower energy width of reflectivity spectrum than the host lattice. The maximum transmittance (T) in Fe-

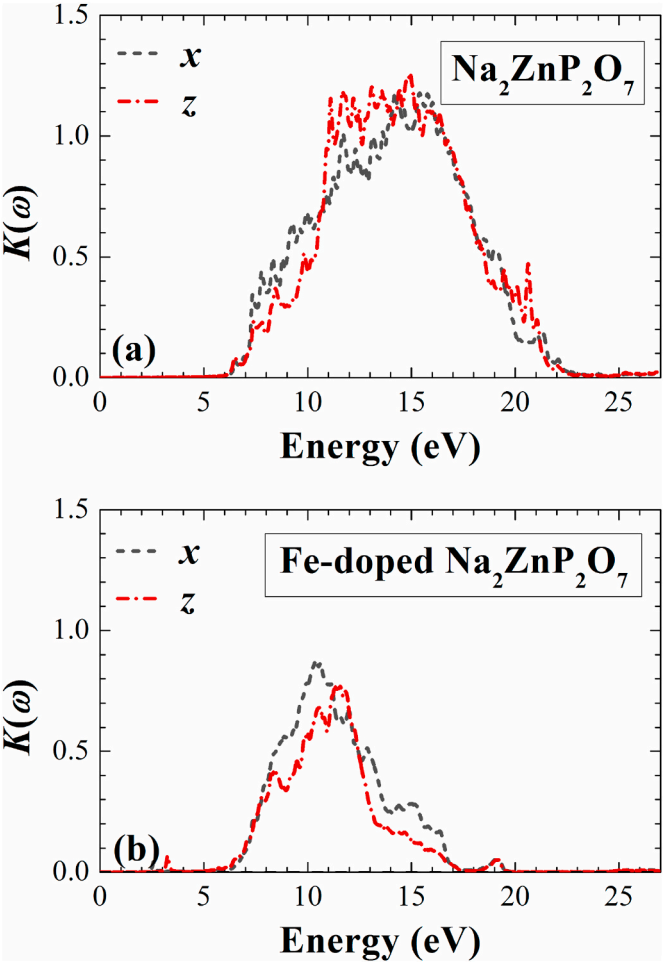

Fig. 10. The calculated extinction index K as a function of photon energy of (a) pure $Na_2ZnP_2O_7$ host lattice, and (b) Fe-doped $Na_2ZnP_2O_7$ using GGA-PBE + U.

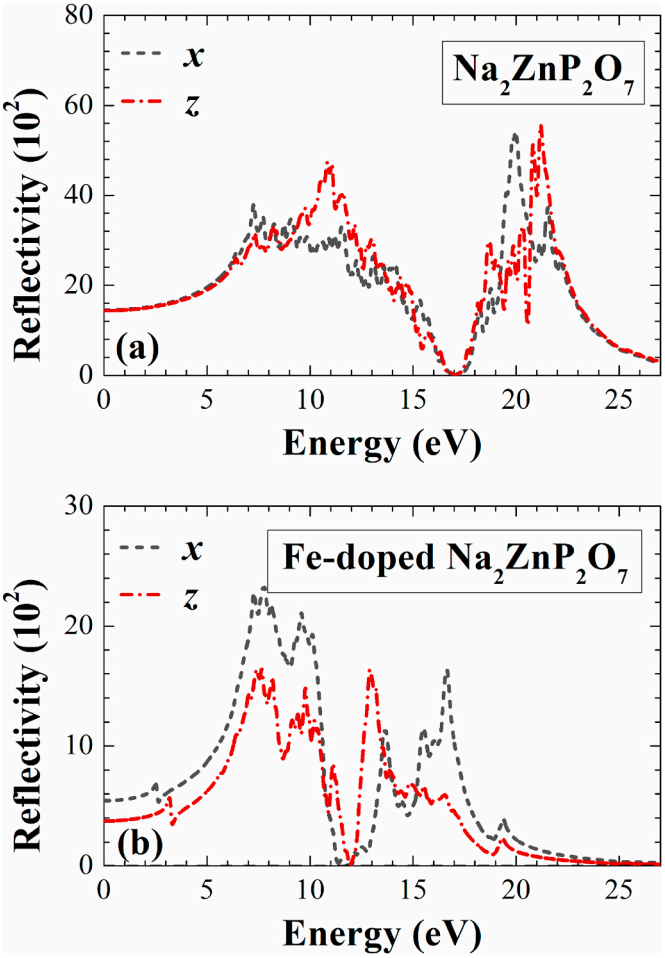

Fig. 11. The calculated optical reflectivity as a function of photon energy of (a) pure $Na_2ZnP_2O_7$ host lattice, and (b) Fe-doped $Na_2ZnP_2O_7$ using GGA-PBE + U.

doped $Na_2ZnP_2O_7$ host lattice is located at 12 eV, which is lower energy than the host lattice, and this indicates that even if the energy is zero, the doped host lattice tends to produce radiation. The static values of the reflection coefficient are 0.058 (≈6%) and 0.04 (4%) for x and z directions, respectively.

In Fig. 12, we present the suggested electronic band structure for optical transitions in pure $Na_2ZnP_2O_7$ and Fe-doped $Na_2ZnP_2O_7$ host lattices. New electronic states associated with the Fe 3d orbitals appear in the band gap for the Fe-doped $Na_2ZnP_2O_7$with low Fe (6.25%) concentration. The d-d transition energy is 0.42 eV and 2.94 eV for the spin up and spin down, respectively. The 3d orbitals split into the doubly degenerated e_g orbital (the lower state), and the triply degenerated t_{2g} orbital (the higher state). In the ground state, all 3d electrons of the Fe atoms occupy the e_g ground state with their spin moments aligned to form the spin-sextet state $^6A_1$. It can be seen that the ground states $^4T_1$ and first excited state $^6A_1$ in spin down configuration of Fe-doped $Na_2ZnP_2O_7$ is considerably higher in energy as compared to spin up configuration.

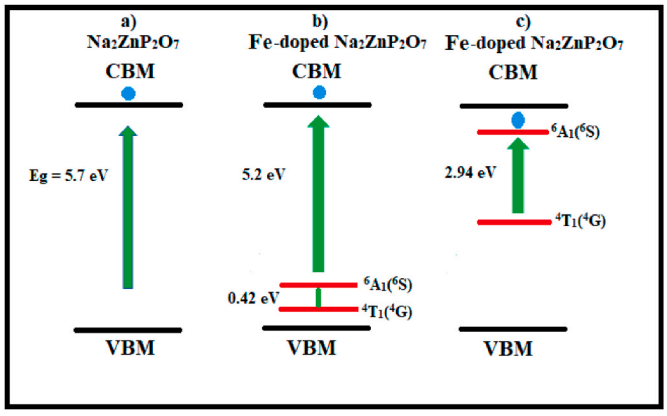

Fig. 12. The suggested band structures for optical transitions in (a) pure $Na_2ZnP_2O_7$ host, (b) Fe-doped $Na_2ZnP_2O_7$ in the spin up direction and (c) $Na_2ZnP_2O_7$ in the spin down direction.

4. Conclusion

The DFT calculations with spin polarization expanded in plane-wave Quantum-ESPRESSO package with both ultrasoft and norm-conserving Vanderbilt pseudopotentials are used to describe electron-ion interactions on pristine and Fe doped $Na_2ZnP_2O_7$. We applied the GGA-PBE functional for the structural optimization and energetic properties to determine the ground state. The electronic and optical properties of the host lattice and Fe doped $Na_2ZnP_2O_7$ were computed using GGA-PBE + U functional. Full geometrical optimization was performed for $Na_2ZnP_2O_7$ host lattice, $Na_{32}Zn_{16}P_{32}O_{112}$ super-cell and $Na_2Zn_{0.937}Fe_{0.0625}P_2O_7$ doped super-cell. An overall agreement of the calculated crystal parameters (a, c) of the host $Na_2ZnP_2O_7$ tetragonal structure with available theoretical and experimental results was observed. From the optimized lattice constants of doped systems, it is observed that the Fe

doped $Na_2ZnP_2O_7$ host lattice results in small volume increase. This is attributed to the close ionic radii of Zn to the Fe. Also, the lattice parameters show no significant major lattice distortion from Fe doping at Zn site in $Na_2ZnP_2O_7$ host lattice compared to the pristine. The formation energy of the undoped and all doped systems are calculated. The formation energy of the pure $Na_2ZnP_2O_7$ host lattice is found to be negative. This means that the formation of this structure is possibly from its elemental constituents and for the Fe-doped $Na_2ZnP_2O_7$, we found it to be thermodynamically favorable. The electronic band structure is computed using the GGA-PBE + U approximations for the $Na_2ZnP_2O_7$ host. We found that both the maximum of valence band (VBM) and the minimum of conduction band (CBM) are situated at the gamma point (Γ → Γ) of the Brillouin zone, which confirms the direct band gap nature of the $Na_2ZnP_2O_7$ host. The computed band gap value of the host lattice is about 5.7 eV, which is in consistent with previous theoretical studies.

Authorship statement

Conception and design of study: Houssam Eddine Hailouf, L. Gacem, A. Gueddim, K.O. Obodo; acquisition of data: Houssam Eddine Hailouf, B. Bouhafs; analysis and/or interpretation of data: Houssam Eddine Hailouf, K.O. Obodo L. Gacem. Drafting the manuscript: Houssam Eddine Hailouf, K.O. Obodo, A. Gueddim, Ali H. Reshak; revising the manuscript critically for important intellectual content: A. Gueddim, B. Bouhafs, Ali H. Reshak. Approval of the version of the manuscript to be published (the names of all authors must be listed): Houssam Eddine Hailouf, L. Gacem, A. Gueddim, Ali H. Reshak, K.O. Obodo, and B. Bouhafs.

Declaration of competing interest

The authors declare that they have no known competing financial interests or personal relationships that could have appeared to influence the work reported in this paper.

Data availability

No data was used for the research described in the article.

Acknowledgements

This work was supported by the Directorate-General for Scientific Research and Technological Development (DGRSDT) of Algeria. We thank the Centre for High Performance Computing (CHPC) in Cape Town, South Africa for computational resources and HySA-Infrastructure Centre of Competence, Faculty of Engineering, North–West University for their financial support. Also, the Materials Science and Informatics Laboratory, Faculty of Science, University of Djelfa is acknowledged for their resources provided, support and the assistance given.

References

[1] K. Biswas, M.-H. Du, Energy transport and scintillation of cerium-doped elpasolite Cs_2LiYCl_6: hybrid density functional calculations, Phys. Rev. B 86 (2012), 014102.
[2] M.-H. Du, K. Biswas, Electronic structure engineering of elpasolites: case of Cs_2AgYCl_6, J. Lumin. 143 (2013) 710–714.
[3] J. Zhang, X. Wu, J. Zhu, Q. Ren, Luminescence properties of a novel $CaLa_4Si_3O_{13}$: Sm^{3+} phosphor for white light emitting diodes, Opt Commun. 332 (2014) 223–226.
[4] G. Dillip, P.M. Kumar, B.D.P. Raju, S. Dhoble, Synthesis and luminescence properties of a novel $Na_6CaP_2O_9$: Sm^{3+} phosphor, J. Lumin. 134 (2013) 333–338.
[5] M. Beltaif, M. Dammak, M. Megdiche, K. Guidara, Synthesis, optical spectroscopy and Judd–Ofelt analysis of Eu^{3+} doped $Li_2BaP_2O_7$ phosphors, J. Lumin. 177 (2016) 373–379.
[6] M. Hassairi, A.G. Hernández, T. Kallel, M. Dammak, D. Zambon, G. Chadeyron, A. Potdevin, D. Boyer, R. Mahiou, Spectroscopic properties and Judd–Ofelt analysis of Eu^{3+} doped $GdPO_4$ nanoparticles and nanowires, J. Lumin. 170 (2016) 200–206.
[7] Z. Yahiaoui, M. Hassairi, M. Dammak, Synthesis and optical spectroscopy of YPO_4: Eu^{3+} orange–red phosphors, J. Electron. Mater. 46 (2017) 4765–4773.
[8] M. Hassairi, M. Dammak, D. Zambon, G. Chadeyron, R. Mahiou, Red–green–blue upconversion luminescence and energy transfer in $Yb^{3+}/Er^{3+}/Tm^{3+}$ doped YP_5O_{14} ultraphosphates, J. Lumin. 181 (2017) 393–399.
[9] M. Fhoula, M. Dammak, Optical spectroscopy and Judd-Ofelt analysis of Eu^{3+} doped in $Na_2ZnP_2O_7$ with high thermal stability for display applications, J. Lumin. 223 (2020), 117193.
[10] G. Mayr, A novel metal-dye detection system permits picomolar-range hplc analysis of inositol polyphosphates from non-radioactively labelled cell or tissue specimens, Biochem. J. 254 (1988) 585–591.
[11] P. Bonnet, J. Millet, Catalytic properties of iron phosphate-based catalysts containing $Fe_2(PO_3OH)P_2O_7$ and α-or β-$Fe_3(P_2O_7)_2$in the oxidative dehydrogenation of isobutyric Acid, J. Catal. 161 (1996) 198–205.
[12] S. Hussain, N. Farooq, A.S. Alkorbi, R. Alsaiari, N.A. Alhemiary, M. Wang, G. Qiao, Polyhedral Co_3O_4@ ZnO nanostructures as proficient photocatalysts for vitiation of organic dyes from waste water, J. Mol. Liq. 362 (2022), 119765.
[13] S. Hussain, X. Yang, M.K. Aslam, A. Shaheen, M.S. Javed, N. Aslam, B. Aslam, G. Liu, G. Qiao, Robust TiN nanoparticles polysulfide anchor for Li–S storage and diffusion pathways using first principle calculations, Chem. Eng. J. 391 (2020), 123595.
[14] S. Hussain, A.J. Khan, M. Arshad, M.S. Javed, A. Ahmad, S.S.A. Shah, M.R. Khan, S. Akram, S. Ali, Z.A. Alothman, Charge storage in binder-free 2D-hexagonal $CoMoO_4$ nanosheets as a redox active material for pseudocapacitors, Ceram. Int. 47 (2021) 8659–8667.
[15] N. Farooq, S. Hussain, A.S. Alkorbi, A.M. Qureshi, M.A. Wattoo, R. Alsaiari, N. A. Alhemiary, A. ur Rehman, Interfaces, Efficient Electrochemical and Photocatalytic Performances of Cu-Doped $Ba_xAl_xO_3$ Nanocomposites, Surfaces Interfaces, 2022, 102116.
[16] M. Brik, I. Sildos, V. Kiisk, Calculations of physical properties of pure and doped crystals: ab initio and semi-empirical methods in application to $YAlO_3$:Ce^{3+} and TiO_2, J. Lumin. 131 (2011) 396–403.
[17] K.O. Obodo, L.L. Noto, S.J. Mofokeng, C.N. Ouma, M. Braun, M.S. Dhlamini, Influence of Tm, Ho and Er dopants on the properties of Yb activated $ZnTiO_3$ perovskite: a density functional theory insight, Mater. Res. Express 5 (2018), 106202.
[18] K.O. Obodo, C.N. Ouma, G. Gebreyesus, J.T. Obodo, S.O. Ezeonu, B. Bouhafs, DFT + U studies of the electronic and optical properties of ReS_2 mono-layer doped with lanthanide atoms, Mater. Res. Express 6 (2019), 106307.
[19] Y. Hu, R. Han, L. Mei, J. Liu, J. Sun, K. Yang, J. Zhao, Materials today energy, Mater. Today 19 (2021), 100608.
[20] S. Hussain, N. Ullah, Y. Zhang, A. Shaheen, M.S. Javed, L. Lin, S.B. Shah, G. Liu, G. Qiao, One-step synthesis of unique catalyst Ni_9S_8@C for excellent MOR performances, Int. J. Hydrogen Energy 44 (2019) 24525–24533.
[21] S. Hussain, M.S. Javed, S. Asim, A. Shaheen, A.J. Khan, Y. Abbas, N. Ullah, A. Iqbal, M. Wang, G. Qiao, Novel gravel-like $NiMoO_4$ nanoparticles on carbon cloth for outstanding supercapacitor applications, Ceram. Int. 46 (2020) 6406–6412.
[22] A.A. Setlur, E.V. Radkov, C.S. Henderson, J.-H. Her, A.M. Srivastava, N. Karkada, M.S. Kishore, N.P. Kumar, D. Aesram, A. Deshpande, Energy-efficient, high-color-rendering LED lamps using oxyfluoride and fluoride phosphors, Chem. Mater. 22 (2010) 4076–4082.
[23] B.V. Kumar, M. Vithal, Luminescence (M= Mn^{2+}, Cu^{2+}) and ESR (M= Gd^{3+}, Mn^{2+}, Cu^{2+}) of $Na_2ZnP_2O_7$: M, Physica B 407 (2012) 2094–2099.
[24] S.L. Dudarev, G.A. Botton, S.Y. Savrasov, C. Humphreys, A.P. Sutton, Electron-energy-loss spectra and the structural stability of nickel oxide: an LSDA+ U study, Phys. Rev. B 57 (1998) 1505.
[25] P. Giannozzi, S. Baroni, N. Bonini, M. Calandra, R. Car, C. Cavazzoni, D. Ceresoli, G.L. Chiarotti, M. Cococcioni, I. Dabo, Quantum Espresso: a modular and open-source software project for quantum simulations of materials, J. Phys.-Condens. Mat. 21 (2009), 395502.
[26] D. Vanderbilt, Soft self-consistent pseudopotentials in a generalized eigenvalue formalism, Phys. Rev. B 41 (1990) 7892.
[27] D. Hamann, Optimized norm-conserving Vanderbilt pseudopotentials, Phys. Rev. B 88 (2013), 085117.
[28] K. Laasonen, A. Pasquarello, R. Car, C. Lee, D. Vanderbilt, Car-Parrinello molecular dynamics with Vanderbilt ultrasoft pseudopotentials, Phys. Rev. B 47 (1993), 10142.
[29] J.P. Perdew, K. Burke, M. Ernzerhof, Generalized gradient approximation made simple, Phys. Rev. Lett. 77 (1996) 3865.
[30] M. Cococcioni, S. De Gironcoli, Linear response approach to the calculation of the effective interaction parameters in the LDA+ U method, Phys. Rev. B 71 (2005), 035105.
[31] J.D. Head, M.C. Zerner, A Broyden—fletcher—Goldfarb—shanno optimization procedure for molecular geometries, Chem. Phys. Lett. 122 (1985) 264–270.
[32] H.J. Monkhorst, J.D. Pack, Special points for Brillouin-zone integrations, Phys. Rev. B 13 (1976) 5188.
[33] H.E. Hailouf, L. Gacem, A. Gueddim, K. Obodo, B. Bouhafs, DFT studies on the structural, electronic, and optical properties of $Na_2ZnP_2O_7$ compound, Mater. Today Commun. 29 (2021), 102868.
[34] M. Fhoula, M. Dammak, Optical spectroscopy of thermal stable $Na_2ZnP_2O_7$: Sm^{3+}/(Li^+, K^+) phosphors, J. Lumin. 210 (2019) 1–6.
[35] S. Zerroug, A. Gueddim, N. Bouarissa, Composition dependence of fundamental properties of $Cd_{1-x}Co_xTe$ magnetic semiconductor alloys, J. Comput. Electron. 15 (2016) 473–478.
[36] N. Bouarissa, A. Gueddim, H. Algarni, M.A. Khan, Phase transition, band structure, optical spectra and magnetic moment of MnO magnetic material upon compression, Eur. Phys. J. B 94 (2021) 1–12.

[37] H. Fujiwara, Spectroscopic Ellipsometry: Principles and Applications, John Wiley &, Sons, 2007.
[38] K. Sturm, Electron energy loss in simple metals and semiconductors, Adv. Phys. 31 (1982) 1–64.
[39] A. Bouarissa, A. Gueddim, N. Bouarissa, H. Maghraoui-Meherzi, Optical response and magnetic moment of MoS_2 material, Optik 208 (2020), 164080.
[40] D.R. Penn, Wave-number-dependent dielectric function of semiconductors, Phys. Rev. B 128 (1962) 2093.
[41] E. Esakkiraj, S.S.A. Kadhar, J. Henry, K. Mohanraj, S. Kannan, S. Barathan, G. Sivakumar, Optostructral and vibrational characteristics of Cu:CdS nanoparticles by precipitation method, Optik 124 (2013) 5229–5231.
[42] M.J.I. Khan, S. Babar, A. Nabi, A.M. Rana, M. Iqbal, S.U. Rehman, J. Ahmad, Theoretical studies of optical properties of Cu doped rocksalt CdS, J. Alloys Compd. 695 (2017) 3605–3611.
[43] J. Hasanzadeh, S.F. Shayesteh, Luminescence of doped CdS nanocrystals: effect of doping and capping agent, Opt. Appl. 41 (2011) 921–928.
[44] M. Petrova, V. Popova, Phase relationships in the $Na_2ZnP_2O_7$–$LiKZnP_2O_7$ system, Glass Phys. Chem. 43 (2017) 380–383.
[45] F.R. Chowdhury, S. Choudhury, F. Hasan, T. Begum, Optical properties of undoped and indium-doped tin oxide thin films, J. Bangladesh Acad. Sci. 35 (2011) 99–111.